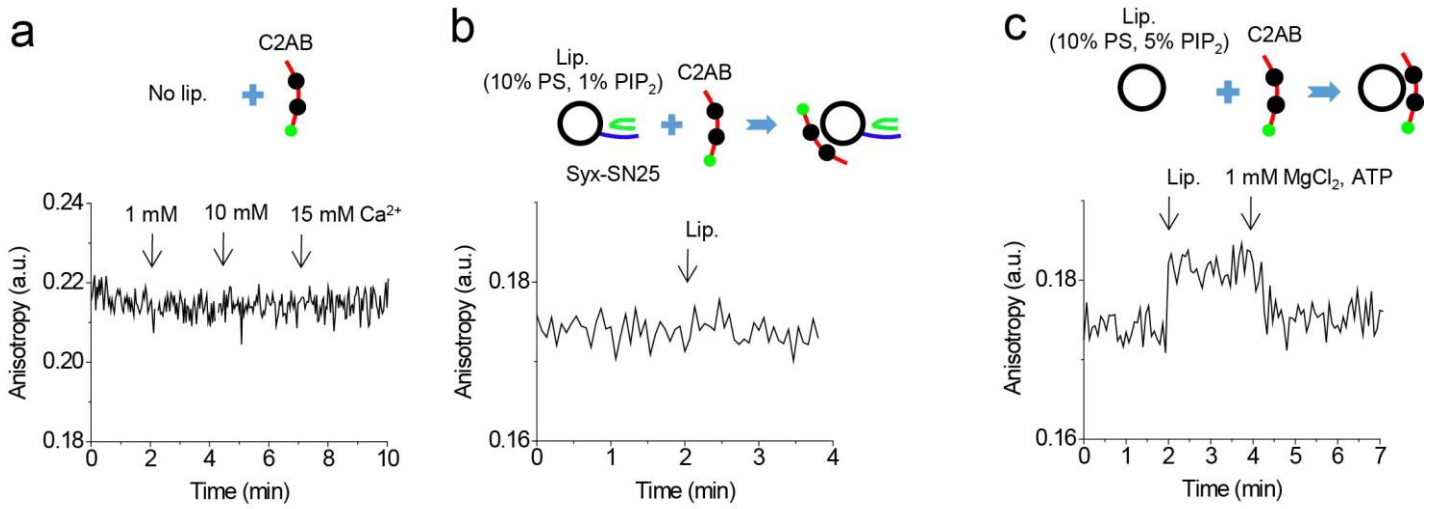

Supplementary Figure 1

High PIP_2 concentrations but no SNAREs are required for Ca^{2+}-independent binding of the C2AB domain.

A labeled variant of the C2AB fragment (Syt_{97-421}, Alexa Fluor 488-labeled at S342C) was used to monitor binding to liposomes (Lip.) by fluorescence anisotropy. 50 μM EGTA was included in all incubations. (**a**) Increasing Ca^{2+} concentration from 1 mM to 15 mM had no effects on anisotropy signal in the absence of liposomes. (**b**) No binding was observable to liposomes containing 1% PIP_2 and the Q-SNARE complex consisting of full-length syntaxin-1A (1-288) and SNAP-25A (Syx-SN25). (**c**) Binding was observable to protein-free liposomes containing 5% PIP_2,, which was reversed by the addition of 1 mM $MgCl_2$/ATP. a.u., arbitrary unit.

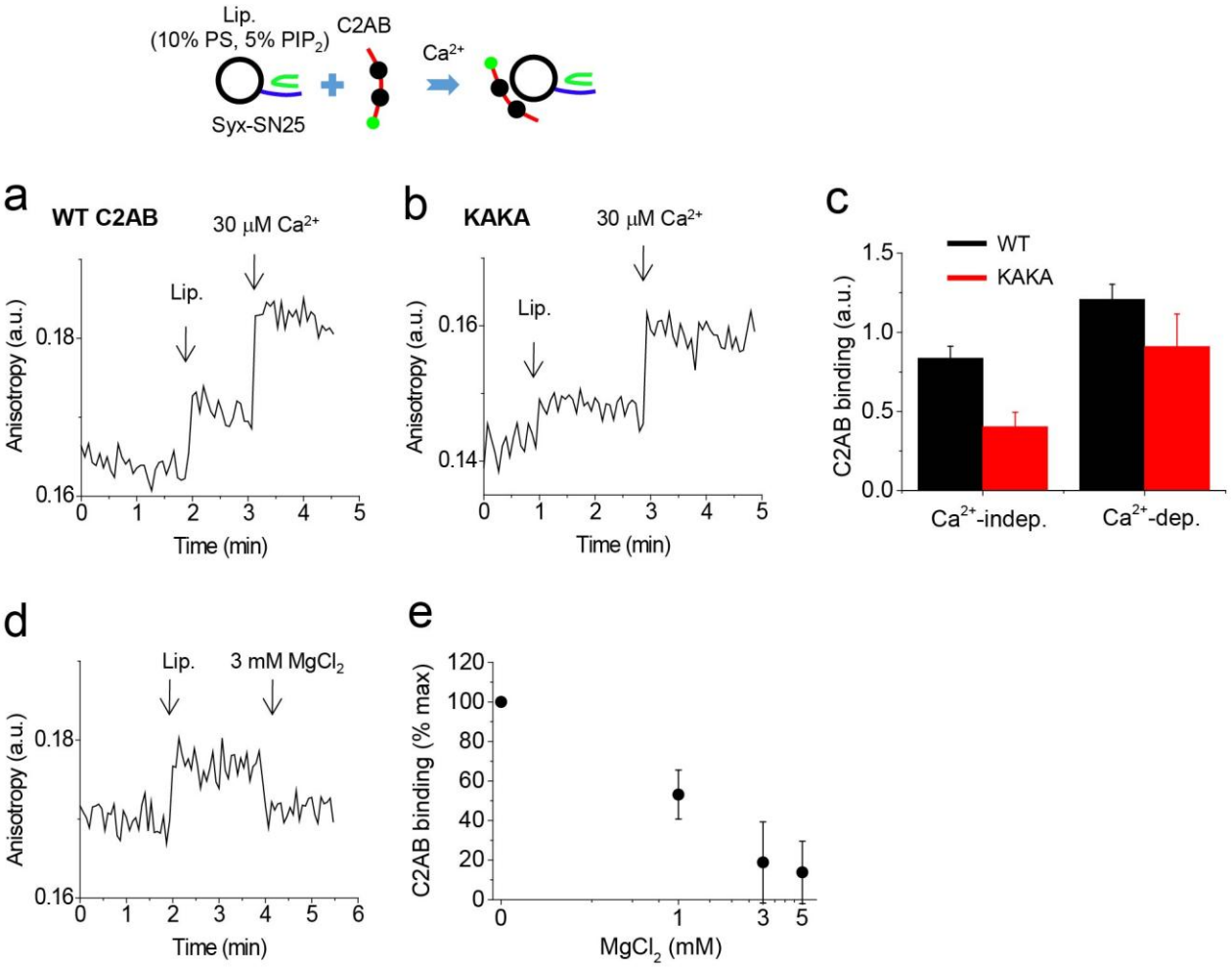

Supplementary Figure 2

Inhibitory effect of Mg^{2+} on Ca^{2+}-independent binding of the C2AB to liposomes.

Fluorescence anisotropy as given in **Supplementary Fig.** 1 for Ca^{2+}-independent binding of the C2AB. (**a-c**) Liposomes (Lip.) and 30 μM free Ca^{2+} were subsequently added to observe Ca^{2+}-independent and Ca^{2+}-dependent binding of C2AB domain, respectively. Mg^{2+} and ATP were absent in this reaction. WT, wild-type C2AB; KAKA, a mutant containing alanine substitutions of two cationic lysine residues in the polybasic region (K326A and K327A). (**c**) C2AB binding was plotted as a net change of anisotropy signal (no $MgCl_2$). (**d,e**) Increasing $MgCl_2$ concentrations reduced Ca^{2+}-independent binding of C2AB domain. (**e**) C2AB binding was presented as percentage of maximum value of C2AB binding in the absence of Mg^{2+}. Data for **c,e** are mean ± SD (n=4~5).

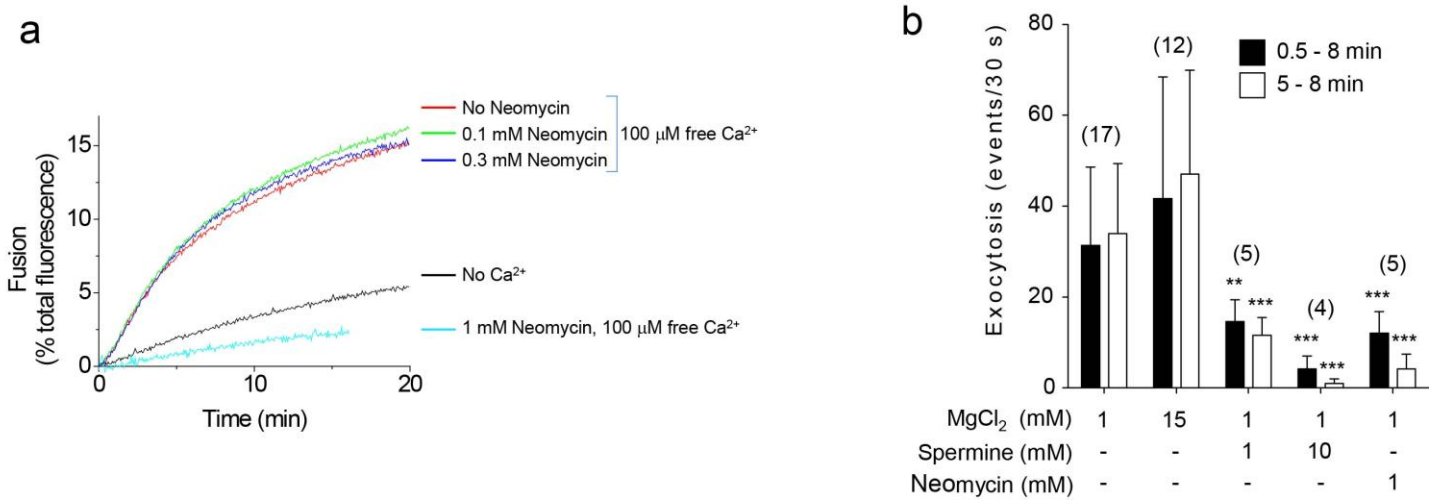

Supplementary Figure 3

Effects of Mg^{2+}, spermine and neomycin on exocytosis of chromaffin granules (CGs).

(a) CG fusion using a lipid-mixing assay. Purified native CGs were incubated with proteoliposomes reconstituted with a stabilized Q-SNARE complex (see **Fig. 1** for details). The free Ca^{2+} concentration was adjusted to 100 μM in the presence of 1 mM $MgCl_2$ and 3 mM ATP using the Maxchelator simulation program (http://maxchelator.stanford.edu). ATP was also included in control (without Ca^{2+}). (**b**) Chromaffin cells were patched with internal solutions containing 50 μM free Ca^{2+} and different concentrations of Mg^{2+}, spermine, or neomycin. All solutions except 15 mM $MgCl_2$ solution contained 1 mM $MgCl_2$. The exocytotic events were detected by a carbon fiber microelectrode and the number of events within 30 s-time window was counted over 8 min. Average rate of exocytosis was analyzed as events per 30 s by counting exocytotic events for 7.5 min (0.5 - 8 min after whole-cell patch clamping). To evaluate the effect of the cations after equilibrium between the patch pipette and cytoplasm, we additionally analyzed the time period between 5 and 8 min whole-cell patch clamping (for 3 min). Number of cells measured was indicated in brackets. ** $P < 0.01$ and *** $P < 0.001$ compared to control (1 mM $MgCl_2$) without spermine or neomycin.

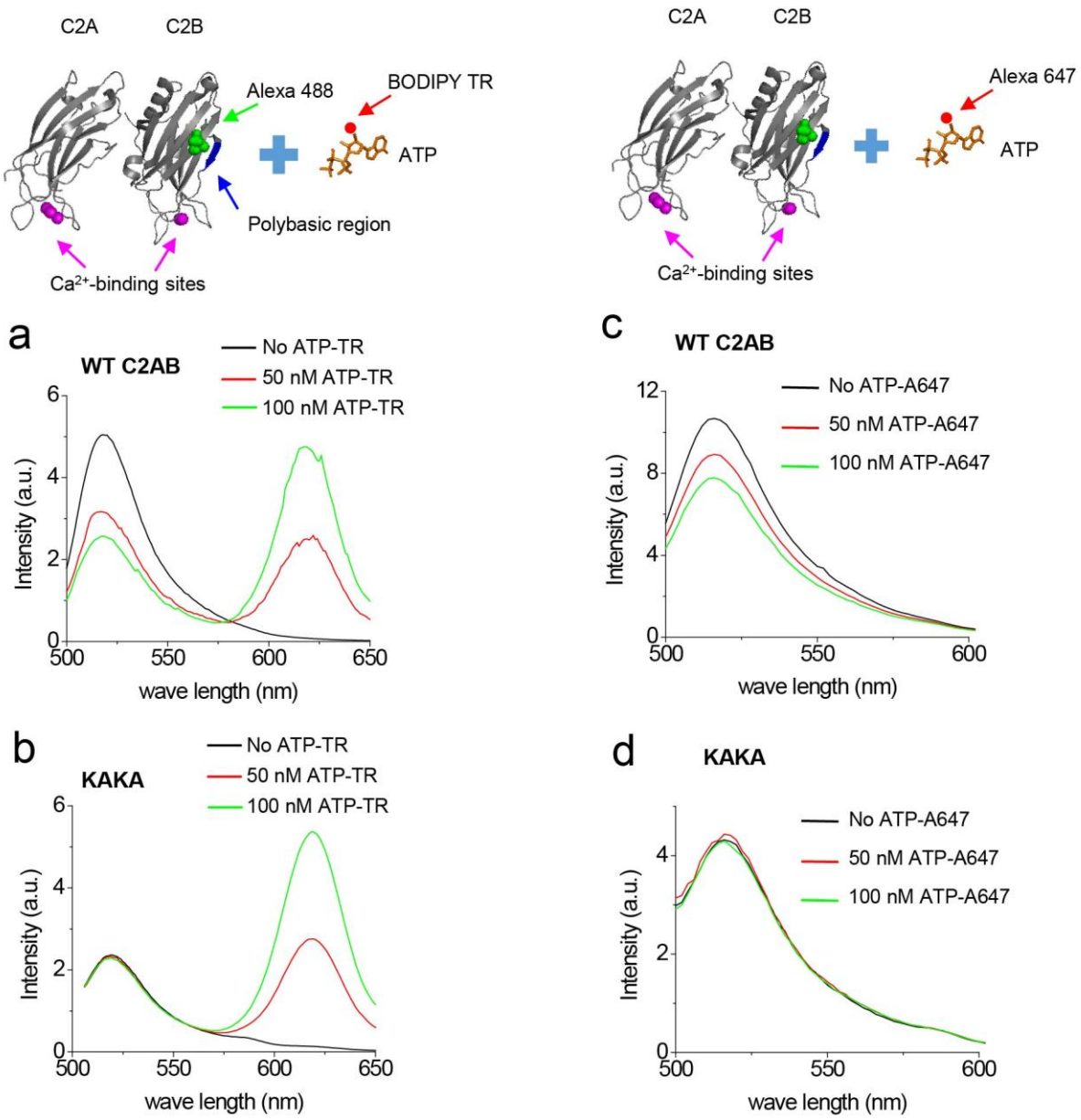

Supplementary Figure 4

Direct interaction of ATP with the polybasic region of the C2B domain.

(**a,b**) FRET measurements in which the C2AB fragment (Syt_{97-421}) and ATP were labeled with Alexa Fluor 488 at S342C (green) and BODIPY Texas Red (red) as a donor and an acceptor, respectively (see **Online Methods** for details). Donor fluorescence was quenched by increasing BODIPY Texas Red-labeled ATP concentrations (**a**), whereas no quenching was observed with the KAKA-mutant (**b**). The fluorescence at 620 nm was from BODIPY Texas Red-ATP. Polybasic region is shown in blue and Ca^{2+} in magenta. (**c,d**) Binding was also observed when ATP labeled with a different dye (Alexa Fluor 647) was used. Shown are emission spectra of donor fluorescence originating from Alexa Fluor 488-labeled C2AB. Mg^{2+} was not included. a.u., arbitrary unit.

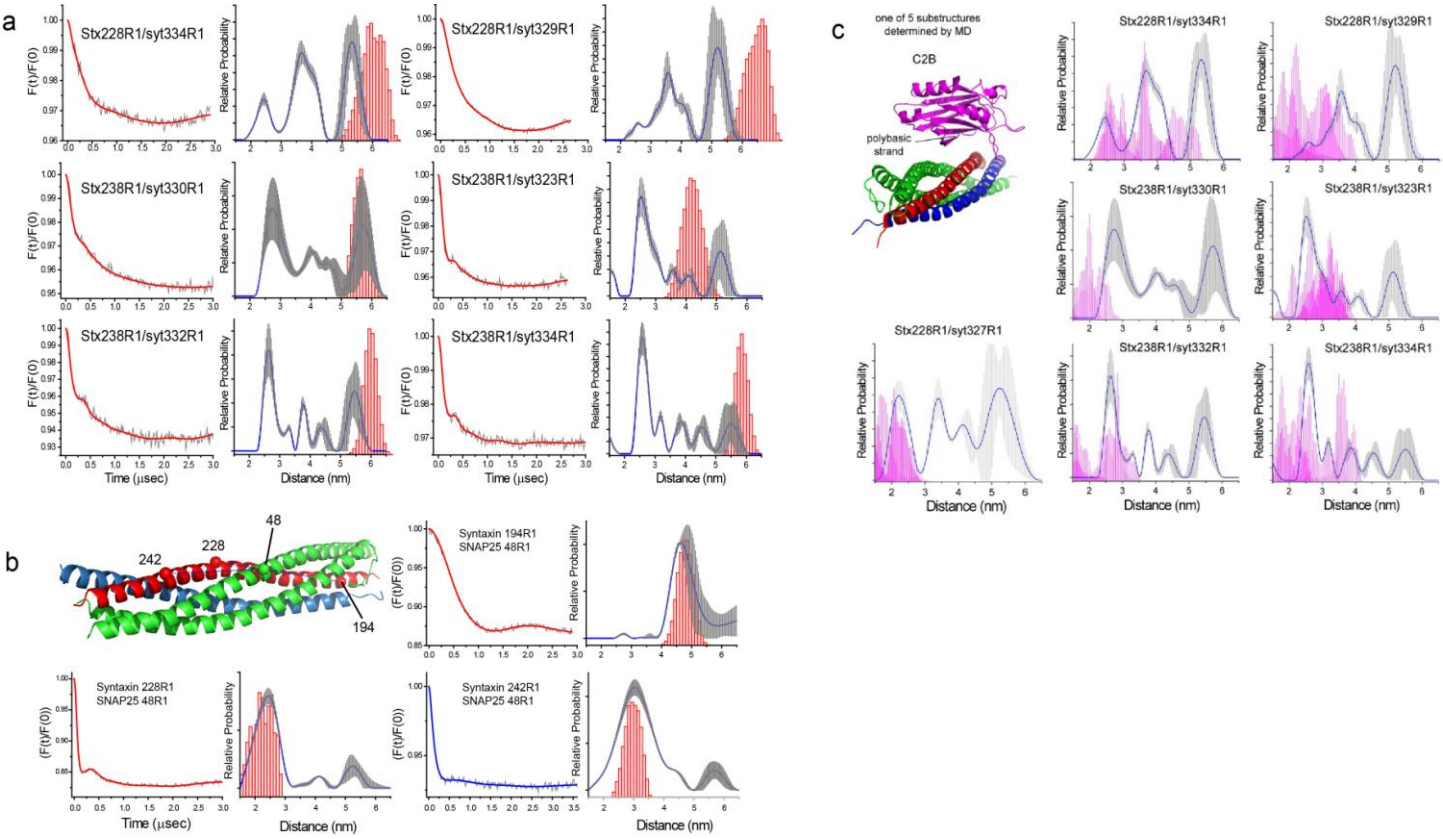

Supplementary Figure 5

Interaction of synaptotagmin-1 and the SNARE complex, monitored by DEER.

(a) Six additional sets of Q-band DEER data obtained from the 1:1 complex formed from C2AB of synaptotagmin-1 (syt1) and the core SNAREs each at a concentration of 50 μM in the presence of Ca^{2+}. The time domain signals (grey traces, left panels) were obtained from a single label in the core SNARE complex at either site 228 or 238 in syntaxin-1A H3 and a second label in the C2B domain of synaptotagmin-1. The distance distribution that yielded the best fit (blue trace) is shown in the corresponding panel to the right. The grey error bars in the distance distributions represent uncertainty due to the background subtraction form factor that produce fits within 15% RMSD of the best fit. The R1 label was incorporated into surface exposed sites of the SNAREs to minimize interference by the label, and efficient labeling of the SNARE proteins was confirmed by mass spectrometry. In every case, the distributions are broad and indicate that there is no specific mode of binding between synaptotagmin-1 and the core SNARE complex under normal ionic strength conditions. No interactions were detected between C2AB and site 211R1 in syntaxin on the N-terminal side of the core SNARE complex. The red histograms represent predictions based on the model generated from single-molecule FRET data (Choi, U.B. *et al*., *Nat Struct Mol Biol* **17**, 318-24, 2010). These predictions are specific to the R1 side chain and take into account the sterically available conformers of R1 at the labeled sites (Hagelueken, G. *et al*., *Appl Magn Reson* **42**, 377-391, 2012). (**b**) DEER measurements were run on three mutants of the core SNARE complex each containing 1 pair of spin labels. One spin label was incorporated into site 48 on SNAP-25A, with a second label at site 194, 228 or 242 of the syntaxin-1A SNARE motif. The time domain DEER signals (grey traces) are shown in the left panels along with the best fits (red traces) using the model-free approach in DeerAnalysis (Jeschke, G. *et al*., *Applied Magnetic Resonance* **30**, 473-498, 2006). The corresponding panels on the right show the experimental distance distributions that represent the best fits (blue traces) to the data. Also shown (grey error bars) is the uncertainty in the distribution based upon variation in the background subtraction form that produces a fit within 15% RMSD of the best fit. The red histograms in the distribution

represent predictions based upon the crystal structure of the core SNARE complex (PDB ID: 1SFC). These were obtained using the PyMol plugin MTSSL Wizard (Hagelueken, G. *et al*., *Appl Magn Reson* **42**, 377-391, 2012). The distances measured between SNAP-25A 48R1 and either syntaxin-1A 194R1 or 228R1 agree well with the predictions from the crystal structure and indicate that the SNARE complex is well-formed. The last pair in the figure (syntaxin-1A 242R1/SNAP25A 48R1) produced the correct distance, but with a broader distribution than expected, suggesting that C-terminal end of the SNARE complex may have some disorder. (**c**) DEER distributions for the synaptotagmin-1–SNARE interaction plotted along with predictions of distance distributions based upon the 5 MD-derived structures in PDB ID: 2N1T (Brewer, K.D. *et al*., *Nat Struct Mol Biol* **22**, 555-64, 2015). The distribution with the best fit to the DEER data is shown in blue and the grey shading indicates the range of distributions that produce fits within 15% RMSD of the best fit. The histograms (magenta) represent the expected distance distributions generated from the heterogeneous synaptotagmin-1 C2B–SNARE complex included in PDB ID: 2N1T (Brewer, K.D. *et al*., *Nat Struct Mol Biol* **22**, 555-64, 2015). The distributions were calculated from a DFT based rotamer library (Warshaviak, D.T.. *et al*., *J Phys Chem B* **115**, 397-405, 2011) using the program MMM (Polyhach, Y.. *et al*., *Phys Chem Chem Phys* **13**, 2356-66, 2011). In most cases, this MD simulation captures the shorter range of these distributions but fails to capture the longer distance components.

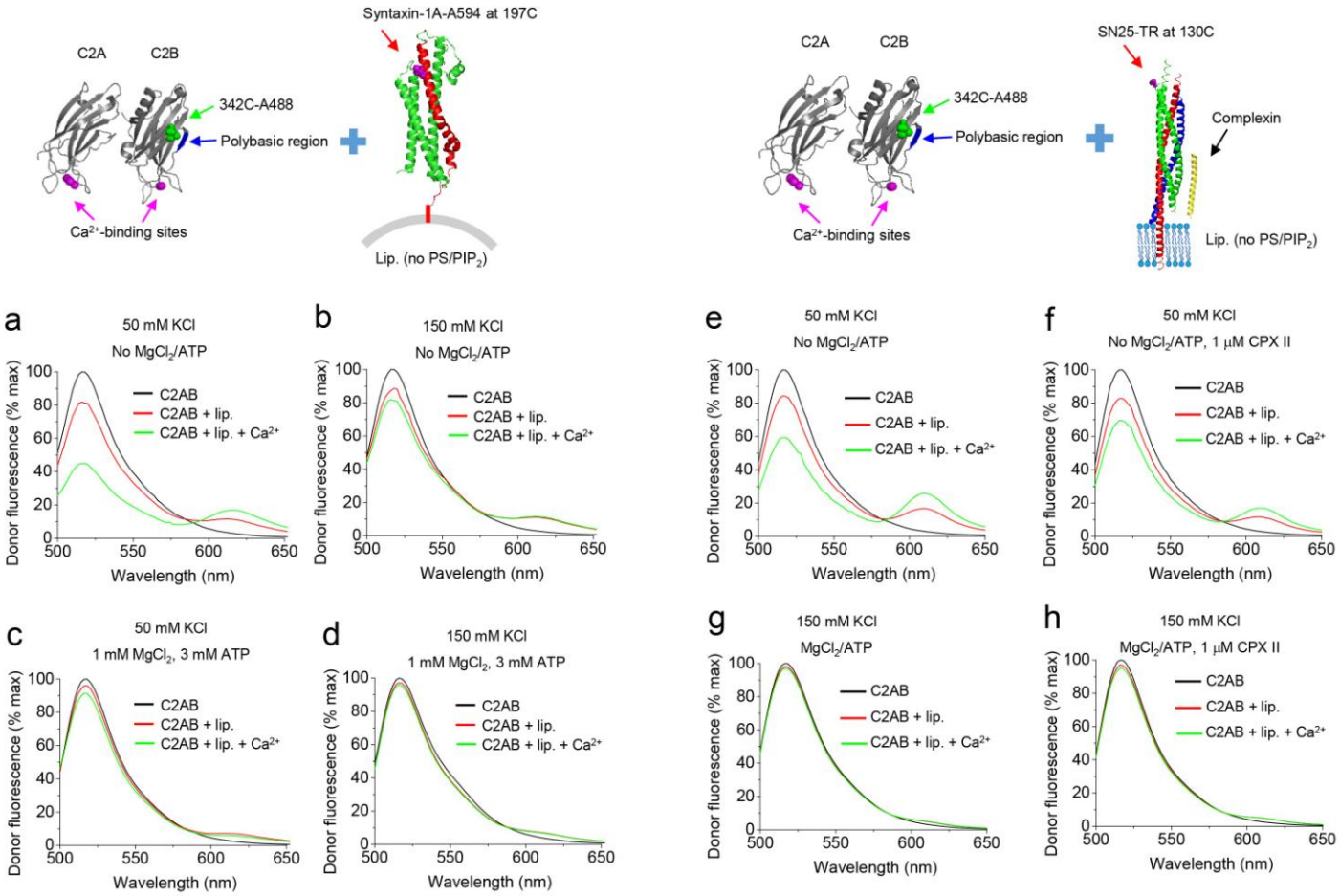

Supplementary Figure 6

No C2AB-SNARE interaction at physiological ionic strength.

(**a-d**) FRET experiments to monitor C2AB binding to syntaxin-1A, in which C2AB fragment and full-length syntaxin-1A (1-288) were labeled with Alexa Fluor 488 at S342C (green) and Alexa Fluor 594 at T197C (magenta) as a donor and an acceptor, respectively. Syntaxin-1A was incorporated in liposomes containing 80% PC and 20% PE (no acidic phospholipids). Full-length syntaxin-1A is shown in green and SNARE motif in red. (**a**) Ca^{2+}-independent and -dependent (1 mM free Ca^{2+}) C2AB binding to syntaxin-1A was exaggerated at low ionic strength (50 mM KCl), compared to normal ionic strength (150 mM KCl, **b**). (**c,d**) C2AB binding to syntaxin-1A was completely disrupted by 1 mM $MgCl_2$ and 3 mM ATP. Donor fluorescence was normalized as percentage of maximum value with C2AB alone. Shown are the typical traces of donor emission fluorescence from 3 to 5 independent experiments. PDB ID: 3C98 for syntaxin-1A. (**e-h**) No C2AB-SNARE interaction even in the presence of complexin II. FRET experiments to monitor C2AB binding to the SNARE complex, in which C2AB fragment and SNAP-25A were labeled with Alexa Fluor 488 at 342C (green) and Texas Red at 130C (magenta) as a donor and an acceptor, respectively. The SNARE complex consisting of synaptobrevin-2 (1-96, blue), SNAP-25A (green), and syntaxin-1A (183–288, red) was incorporated in liposomes containing 80% PC and 20% PE. (**e,f**) Ca^{2+}-independent and -dependent (1 mM free Ca^{2+}) C2AB binding to SNAREs was observed at low ionic strength (50 mM KCl) in the absence or presence of 1 μM complex II. (**g,h**) C2AB binding to SNAREs was not observed at physiological ionic strength (150 mM KCl, 1 mM $MgCl_2$, and 3 mM ATP) regardless of whether complexin II was present or not. Donor fluorescence was normalized as percentage of maximum value with C2AB alone. Structures were visualized with the program PyMOL (PDB ID: 1KIL for complexin and 1SFC for SNARE complex).

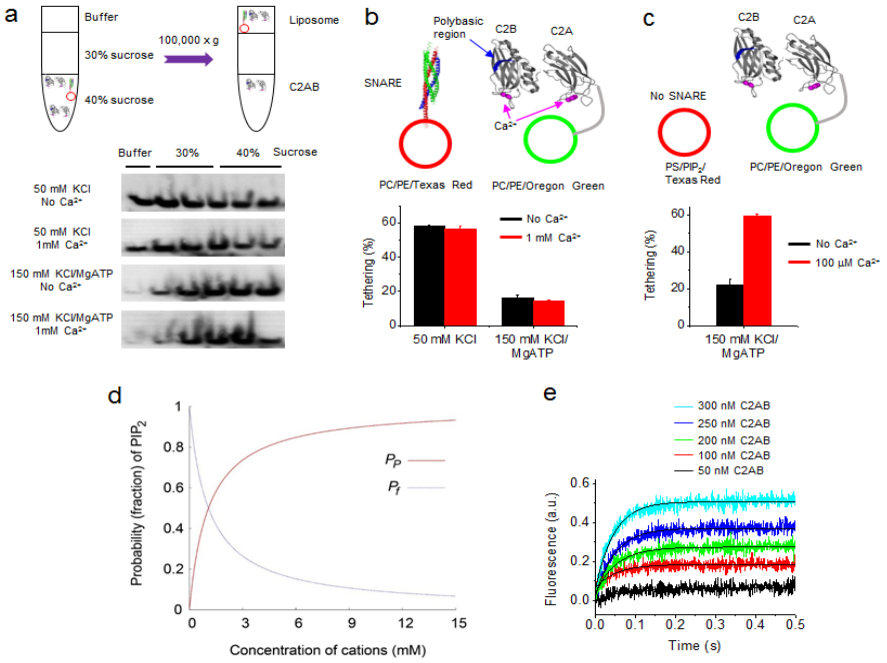

Supplementary Figure 7

No C2AB-SNARE interaction at physiological ionic strength.

(**a**) Liposome co-flotation assay to test the C2AB-SNARE interaction. Physiological ionic environment (150 mM KCl, 1 mM $MgCl_2$, and 5 mM ATP) completely reduced the C2AB interaction with the SNAREs in buffer fraction regardless of whether Ca^{2+} was present or not. (**b,c**) Fluorescence cross-correlation spectroscopy (FCCS) to test liposome tethering by proteins. (**b**) Incubation of liposomes (synaptotagmin-1, 80% PC, 19% PE, and 1% Oregon Green-DHPE) with 1% Texas Red-containing liposomes which incorporate the SNARE complex (full-length syntaxin-1A, SNAP-25A, and soluble synaptobrevin-2 (aa 49-96)) led to liposome tethering in low ionic strength (50 mM KCl). Physiological ionic strength (150 mM KCl/1 mM $MgCl_2$/5 mM ATP) reduced the SNARE-synaptotagmin-1 interaction, independently of Ca^{2+}. (**c**) SNARE-free liposomes containing 10% PS, 1% PIP_2, and 1% Texas Red-DHPE (see **Online Methods** for details of lipid composition) was incubated with synaptotagmin-1-containing liposomes. 100 μM Ca^{2+} specifically increased liposome tethering in a physiological ionic strength (150 mM KCl, 1 mM $MgCl_2$, and 5 mM ATP). Data are mean ± SD (n = 3). (**d**) Simulation of PIP_2 by divalent cations. The fractions P_p (screened PIP_2, red line) and P_f (free PIP_2, blue line) are plotted based on parameters given in Supplementary Table 1. (**e**) Kinetics of the C2AB binding to liposome membranes. Averaged time courses of the rhodamine emission at different concentrations of C2AB. Liposomes were rapidly mixed with an equal volume of solutions containing different C2AB concentrations under pseudo-first order conditions. a.u., arbitrary unit.

Parameters	Description	Value	Unit
e_P	Electric potential energy of a screened PIP_2	1.24	eV
e_S	Electric potential energy of a screened PS	1.24	eV
k_B	Boltzmann constant	$^{*}1.38 \times 10^{-23}$	J/K
T	Absolute temperature	$^{*}3.10 \times 10^{2}$	K
V_P	Effective volume of a PIP_2	7.29×10^{-18}	mL
V_S	Effective volume of a PS	5.36×10^{-18}	mL
C_P	Total concentration of PIP_2	$^{\dagger}1.00 \times 10^{-4}$	mM
C_S	Total concentration of PS	$^{\dagger}1.00 \times 10^{-3}$	mM
k	Maximum effective Ca^{2+} concentration (trans-binding)	5.08×10^{-2}	mM
l	Ca^{2+} concentration corresponding to $k/2$	1.97×10^{-1}	mM
m	Maximum effective Ca^{2+} concentration (cis-binding)	2.60×10^{-1}	mM
n	Ca^{2+} concentration corresponding to $m/2$	2.93	mM
K_{PC}	Equilibrium dissociation constant of PIP_2 binding, depending on Ca^{2+}	5.43×10^{-7}	mM^2
K_{SC}	Equilibrium dissociation constant of PS binding, depending on Ca^{2+}	8.90×10^{-6}	mM^2
n	Exponent of Ca^{2+} cooperativity	$^{*}1.85$	(unitless)
a_C	Proportionality constant for PIP_2-binding, depending on Ca^{2+}	1.21×10^{2}	% max
b_C	Proportionality constant for PIP_2-mediated fusion, depending on Ca^{2+}	4.90×10^{2}	% control
a_M	Proportionality constant for PIP_2-binding, depending on Mg^{2+}	1.64×10^{2}	% max
b_M	Proportionality constant for PIP_2-mediate fusion, depending on Mg^{2+}	6.42×10^{2}	% control
c_C	Proportionality constant for PS-binding, depending on Ca^{2+}	2.96×10^{2}	% max
d_C	Proportionality constant for PS-binding in fusion, depending on Ca^{2+}	8.07×10^{2}	% control

Supplementary Table 1

Parameters for the PIP_2 screening model. Parameter values marked with * and † have been determined from the experimental conditions and from literature (Augustine, G.J. & Neher, E., *J Physiol* **450**, 247-71, 1992; Mohr, P.J., Taylor, B.N. & Newell, D.B. *Rev Mod Phys* **84**, 1527-605, 2012), respectively. Other parameters have been obtained from fitting the experimental data.